

AsymRnR: Video Diffusion Transformers Acceleration with Asymmetric Reduction and Restoration

Wenhao Sun Rong-Cheng Tu* Jingyi Liao Zhao Jin Dacheng Tao*

Nanyang Technological University

{wenhao006, rongcheng.tu, jingyi012, zhao.jin, dacheng.tao}@ntu.edu.sg

Abstract

Video Diffusion Transformers (DiTs) have demonstrated significant potential for generating high-fidelity videos but are computationally intensive. Existing acceleration methods include distillation, which requires costly retraining, and feature caching, which is highly sensitive to network architecture. Recent token reduction methods are training-free and architecture-agnostic, offering greater flexibility and wider applicability. However, they enforce the same sequence length across different components, constraining their acceleration potential. We observe that intra-sequence redundancy in video DiTs varies across features, blocks, and denoising timesteps. Building on this observation, we propose Asymmetric Reduction and Restoration (AsymRnR), a training-free approach to accelerate video DiTs. It offers a flexible and adaptive strategy that reduces the number of tokens based on their redundancy to enhance both acceleration and generation quality. We further propose matching cache to facilitate faster processing. Integrated into state-of-the-art video DiTs, AsymRnR achieves a superior speedup without compromising the quality.

1. Introduction

Recent progress in video generation has been largely propelled by innovations in diffusion models [18, 47, 49]. Building on these developments, the Diffusion Transformer (DiT) [39] has achieved state-of-the-art results across a range of generative tasks [46, 52, 58, 64, 68]. This success largely stems from its ability to model global receptive fields within each block effectively. However, the generation speed of video DiTs remains a significant bottleneck, often taking minutes or even hours to produce just a few seconds of clip [27, 53, 54, 65]. A primary factor resulting in this slowdown is the high computational cost of modeling global attention over inherently long video sequences, which motivates our pursuit of more efficient acceleration strategies.

*Corresponding authors

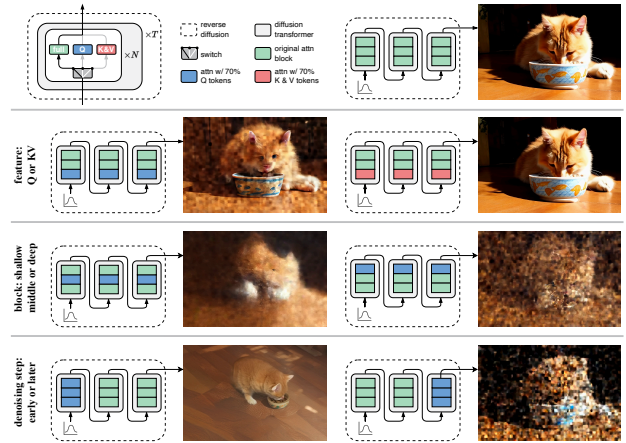


Figure 1. **Impact of perturbing different components in a video DiT** [65]. **Green blocks** represent unmodified original attention blocks. **Blue blocks** represent attention blocks where 30% of the query tokens are randomly replaced, allowing only the remaining 70% to contribute to the output. **Red blocks** represent the same perturbation applied to key and value tokens. The comparison includes: 1) Perturbing different **features**: Q vs. KV ; 2) Perturbing different **blocks** of DiT: shallow, intermediate vs. deep; 3) Perturbing different **denoising steps**: early vs. later.

Since attention layers are the main contributor to the computational complexity of transformers, optimizing these operations has been a long-standing research focus [8, 9, 40, 41, 66]. In vision diffusion models, distillation methods [34, 38, 44, 45, 54] are widely employed to reduce sampling steps and network complexity. However, they require extensive training and impose high computational costs. Feature caching techniques [24, 71, 72] offer an alternative through bypassing computations in certain intermediate layers without altering the network parameters, thus speeding up execution. Nevertheless, such methods are often designed for particular network architectures [27, 36, 73], which limits their applicability to broader scenarios. Another promising avenue is to shorten the length of the token sequence [3, 29].

For example, Token Merging (ToMe) approaches [3, 29] merge highly similar (*i.e.* redundant) tokens to accelerate the image generation in Stable Diffusion (SD) [42].

However, directly extending ToMe methods to video DiTs often results in over-pixelation and distortions (as shown in Fig. 6). We hypothesize that this issue arises from the uniform reduction of attention features across blocks and denoising timesteps, disregarding their varying contributions to the output. To evaluate this assumption, we randomly discarded 30% of tokens from different features, blocks, and denoising timesteps. The visualization in Fig. 1 reveals the following: 1) Perturbations in the query (Q) of early blocks significantly degrade generation quality, whereas similar perturbations in the key (K) and value (V) have a lesser impact. 2) The degradation intensity varies across perturbed blocks, following a hierarchical pattern: shallow blocks > intermediate blocks > deep blocks. 3) Perturbing the Q across all blocks but at specific denoising timesteps show that early-timestep perturbations primarily affect semantic accuracy (*e.g.* temporal motion and spatial layout), while later-timestep perturbations degrade visual details. Prior token reduction methods [3, 23, 29], while more targeted than random reduction strategies, still distribute perturbations uniformly across all components. This uniformity disproportionately affects the most sensitive components, leaving the perturbation tolerance thresholds of less sensitive ones unmet. Consequently, errors in these vulnerable components propagate through the system, degrading overall output quality. This phenomenon mirrors Liebig’s law of the minimum, where *a system’s capacity is constrained by its weakest element, akin to a barrel limited by its shortest stave.*

Inspired by these observations, we propose Asymmetric Reduction and Restoration (AsymRnR) as a plug-and-play approach to accelerate video DiTs without retraining or architectural modifications. The core idea is to asymmetrically reduce the sequence length of the attention sequence before self-attention and then restore the original sequence length for subsequent operations. We also introduce the matching cache, which bypasses unnecessary matching computations to further accelerate. Finally, we propose a reduction schedule that adaptively adjusts the reduction rate to account for nonuniform redundancy across blocks and denoising timesteps. We conducted extensive experiments to evaluate its effectiveness and design choices using the state-of-the-art video DiTs, including CogVideoX [65] 2B and 5B variants. With AsymRnR, these models exhibit noticeable acceleration with negligible quality degradation. We anticipate that our work will contribute to further advancements in efficient video generation.

2. Related Work

2.1. Video Diffusion Networks

Factorized UNet. Video diffusion pioneers [15, 19, 59, 60, 69] adapted the UNet [43] backbone and spatial layers originally developed for image generation. New temporal layers are introduced to capture motion dynamics and enable smooth transitions between frames. Leveraging prior knowledge embedded in the spatial layers, video diffusion methods with factorized 3D UNet backbone have shown promising initial results.

Factorized DiT. With the emergence of DiTs demonstrating efficiency in image diffusion [5, 14], video models also followed the trend toward architecture unification and transitioned to a factorized DiT backbone [27, 36, 73]. This modification leverages optimized low-level operations [8, 9, 40], efficient design practices, and cross-domain training recipes [13, 19]. It also achieves additional compression by processing patches instead of pixels, which is well-suited for long-context video representation. However, these models retain the factorized structure of earlier approaches, inherently limiting their ability to represent highly dynamic objects due to indirect communication between inter-frame pixels across different spatial coordinates.

Global DiT. Advanced video diffusion methods [27, 53, 55, 65] employ a global DiT backbone to address the limitation as mentioned earlier. Specifically, for input tokens $H \in \mathbb{R}^{n \times d}$, the self-attention operation is defined as follows:

$$\begin{aligned} \text{Attn}(H) &= \text{softmax}(QK^T)V \\ &= \text{softmax}((HW_Q)(HW_K)^T)(HW_V), \end{aligned} \quad (1)$$

where $W_Q, W_K, W_V \in \mathbb{R}^{d \times d}$ are the projection matrices, and n represents the sequence length. Certain operations, such as positional embeddings [51] and normalization [1], are omitted here for brevity.

The self-attention operation has a $O(n^2)$ time complexity. For video features, n is typically very large; for instance, a 48-frame (6 seconds at 8 FPS) 640×960 video results in $n = 12 \times 30 \times 45 = 16200$ after VAE [67] ($4 \times 8 \times 8$ downsampling) and patchification ($1 \times 2 \times 2$ downsampling). Our goal is to simplify its calculation to improve efficiency.

2.2. Efficient Diffusion Models

Iterative sampling in diffusion models poses a significant bottleneck for the generation process. Even fast ODE solvers [11, 32, 48, 70, 70] still require around 10 steps, often leading to an inevitable drop in generation quality. Recent methods aim to mitigate this issue by employing step distillation and feature caching to streamline inference.

Step Distillation. Diffusion step distillation studies [38, 44] reduce sampling steps to as few as 4–8. Additionally, ad-

versarial losses are involved to mitigate performance degradation during the distillation process [45]. InstaFlow [31] introduces a integration of Rectify Flow [30] into distillation pipelines, enabling extreme model compression without sacrificing much quality. Consistency Models (CMs) [50] enhance performance in few-step generation by regularizing the ODE trajectories during distillation, ensuring stable and accurate sampling. Latent Consistency Model (LCM) [33] extends this approach to LDMs [42], achieving high performance with few-step generation. Moreover, LCM-LoRA [34] provides an efficient low-rank adaptation [20], enabling the transfer of the pretrained Stable Diffusion variants into 4-step models.

Feature Caching. Recognizing the small variation in high-level features across adjacent denoising steps, studies [6, 16, 35, 62] reuse these features while updating the low-level ones in UNet [43] denoising predictors. T-GATE [71] caches the redundant cross-attention features during the fidelity-improving stage. PAB [72] caches both self-attention and cross-attention features across different broadcast ranges. AdaCache [24] adaptively caches features based on the computational needs of varying contexts.

Despite significant progress, distillation methods require re-training to accommodate new sampling paradigms. Feature caching methods are tightly coupled to specific architectures, necessitating redesign for new architectures. In contrast, our token-level method is training-free, complements many DiT variants, and integrates seamlessly with existing acceleration techniques to further improve efficiency.

2.3. Token Reduction

As research advances in processing long contexts within NLP [28, 63], computer vision [7, 26, 41, 66], and multi-modal tasks [10, 22, 23, 29, 37, 56, 57] using transformers, substantial efforts have focused on reducing sequence length to improve computational efficiency. Most of these methods target discriminative and autoregressive generation tasks, where token reduction is achieved by selectively truncating based on the outputs of preceding layers or steps, with these reductions compounding throughout the process. However, this approach is challenging to apply to dense prediction tasks like diffusion denoising, where the entire sequence must remain restorable.

Token Merging (ToMe) [3] achieves token reduction by merging tokens based on intra-sequence similarity before compute-intensive modules, which has been generalized to image generation with SD [42]. However, directly extending ToMe to video DiTs poses challenges, often leading to excessive pixelation and blurriness. Additionally, calculating similarity for merging is computationally expensive. Our method aims to reap the advantages of token reduction techniques while ensuring stable visual quality.

3. Method

Consider a self-attention layer that processes an input matrix $H \in \mathbb{R}^{n \times d}$, where n is the sequence length and d is the feature dimension. The standard dot-product self-attention first maps H to three matrices, queries $Q \in \mathbb{R}^{n \times d}$, keys $K \in \mathbb{R}^{n \times d}$, and values $V \in \mathbb{R}^{n \times d}$. It then takes the dot product between each query and all keys, followed by applying a softmax function to obtain the weights on value as shown in Eq. (1). This results in a time complexity of $O(n^2)$, which becomes costly for the large n in video generation.

We optimize the self-attention layers in video DiTs by reducing the sequence length n , specifically by pruning redundant tokens to avoid unnecessary computations. Sec. 3.1 introduces the preliminaries and the symmetric reduction-restoration approach. Sec. 3.2 details our asymmetric techniques, offering greater flexibility. Sec. 3.3 proposes matching cache to mitigate the overhead of additional computations. Finally, Sec. 3.4 presents a nonuniform reduction schedule that enhances efficiency by dynamically allocating the reduction budgets.

3.1. Symmetric Reduction and Restoration

Early research [3, 4, 23, 29] explores intra-sequence matching to detect redundant tokens within sequences. These methods reduce the sequence length of attention features symmetrically, treating queries Q and key-value pairs KV indistinguishably. We review these approaches in this section.

Bipartite Soft Matching (BSM). Calculating the naive pairwise similarity between each token and all others to identify redundant tokens and organize their matches among the n tokens is computationally intensive, potentially undermining speed improvements. BSM [4] is introduced to efficiently identify token matches by calculating the similarity between two disjoint subsets: the source subset with size n_1 and the destination subset with size n_2 , where $n = n_1 + n_2$. More precisely, the source token set $\{h_{s_1}, \dots, h_{s_{n_1}}\}$ and the destination token set $\{h_{d_1}, \dots, h_{d_{n_2}}\}$ form a partition of the feature token set $\{h_1, \dots, h_n\}$. Each source token is matched with its most similar destination token and only the top n_r matches, determined by similarity scores, are retained for the following token reduction process. Here n_r is the predefined number of tokens to reduce, and $r = n_r/n$ represents the relative reduction rate.

Partitioning. ToMe [3] splits the image tokens into patches using 2D strides (e.g. 2×2), and randomly adds one token from each patch to the destination set in SD. This design balances randomness and regulation, effectively avoiding gridding and clumping effects. We adopt this design and extend it to 3D strides for video. Specifically, we set the stride length to 2 for both temporal and spatial dimensions.

Symmetric Reduction and Restoration (SymRnR). As

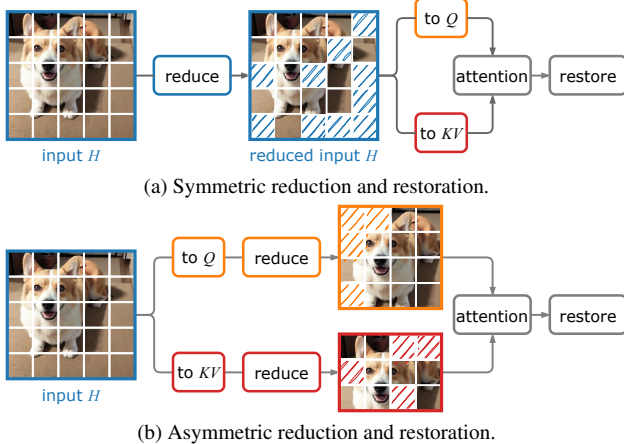


Figure 2. **Overview of symmetric and asymmetric strategies.** They are designed to enhance computational efficiency by reducing the attention sequence length. We use image patches for illustrative purposes.

shown in Fig. 2a, prior works [3, 23, 29] reduce the sequence length of input H (so symmetrically reduce Q and KV), enabling self-attention to operate on a reduced sequence for improved efficiency. To preserve compatibility with diffusion denoising, the compressed tokens are restored by replicating their most similar destination tokens, thereby ensuring the sequence length matches the original input. Formally, the attention operation with general SymRnR applied can be formulated as follows:

$$\text{SymRnR}(H) = \mathcal{R}^{-1} \circ \text{Attn} \circ \mathcal{R}(H), \quad (2)$$

where $\mathcal{R}(\cdot)$ and $\mathcal{R}^{-1}(\cdot)$ represent the reduction and restoration operations, respectively. Notably, this process is lossy, and the resulting error is often substantial in DiT due to its coarse design.

3.2. Asymmetric Reduction and Restoration

In contrast to prior works that emphasize reducing H , we target the reduction of Q and KV , as depicted in Fig. 2b. This approach enables an asymmetric treatment of Q and KV , tailored to their respective contributions to the final output. The attention operation with our Asymmetric Reduction and Restoration (AsymRnR) is formulated as follows:

$$Q' = \mathcal{R}_Q(Q), \quad K', V' = \mathcal{R}_{KV}(K, V), \quad (3)$$

$$\text{AsymRnR}(H) = \mathcal{R}_Q^{-1}(\text{softmax}(Q'(K')^T)V').$$

It is worth noticing that K and V must share the same reduction scheme due to their one-to-one correspondence, whereas Q can be compressed independently of the other features. The restoration will reverse the reduction applied to Q by the nature of the attention operation. Benefiting from the decoupled design, our method adapts the reduction rate to dif-

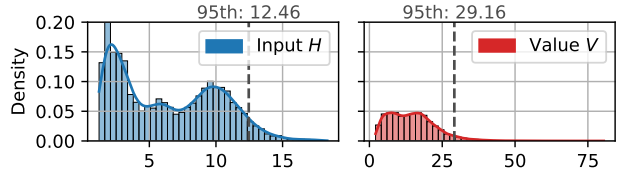


Figure 3. **The distribution of feature Euclidean norms.** The dashed line indicates the 95th percentile. Compared to input H , the value V norm distribution exhibits a longer tail, which can cause distortion when using cosine similarity for matching.

ferent features based on their redundancy, achieving greater speedup without compromising quality in the experiments.

Theoretically, SymRnR and AsymRnR are compatible and can be combined sequentially or in parallel to achieve greater speedup. However, the experiments demonstrate that such integration results in performance degradation, whereas directly scaling the reduction rate of AsymRnR yields superior performance. We focus on AsymRnR and leave their integration to future work.

Similarity Metrics. The attention operation relies on the dot product metric (*i.e.* cosine similarity) for calculating the attention map [12, 25]. Therefore, it is regarded as the standard approach for token similarity in previous works [3, 4, 23, 29]. However, we observed that cosine similarity leads to dark spots and a dim atmosphere in the generated videos, especially when reducing the V . To investigate the root cause of this issue, we visualized the distribution of feature norms in Fig. 3. The norm distributions for V exhibit significantly longer tails than H : a small proportion of tokens showing significantly larger norms. Using cosine similarity disregards the magnitude of these tokens, which can result in matching tokens with greatly different magnitudes, thereby causing instability. To address this issue, we use the (negative) Euclidean distance, which accounts for both the direction and magnitude differences between paired vectors.

3.3. Matching Cache

One drawback of matching-based reduction methods is the additional cost incurred by the matching process during each reduction. Despite using BSM [4], the matching process still significantly negates the speedup achieved in attention.

We observed that the intra-sequence similarity at successive denoising steps exhibits only minor differences as illustrated in Fig. 4. Similar patterns were also observed in the hidden states produced by the denoising network layers [2, 6, 35]. This observation motivates us to cache the matching results over denoising steps, avoiding recalculations and saving computational costs. Formally, matching similarity

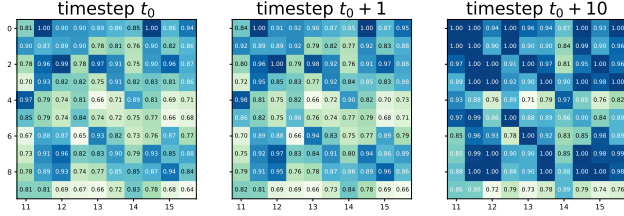


Figure 4. **Heatmap of matching similarity at different denoising timesteps.** The similarities across successive timesteps are nearly identical, but divergence increases with a larger step gap. We propose a matching cache to reuse similarities across successive timesteps, recalculating them only when significant divergence from the cached values occurs.

with caching is defined as:

$$\mathcal{S}^{(t)}(A^{(t)}) = \begin{cases} \text{BSM}(A^{(t)}) & \text{if } t = 1 \pmod{s} \\ \mathcal{S}^{(s \cdot \lfloor t/s \rfloor)} & \text{otherwise} \end{cases}, \quad (4)$$

where $\mathcal{S}^{(t)}$ denotes the matching similarity at reverse diffusion timestep $t \in [1, T]$, $\text{BSM}(\cdot)$ represents the bipartite soft matching [4] mentioned in Sec. 3.1, $A \in \{H, Q, K, V\}$ represents the attention sequences, and s denotes the caching steps. In this way, the matching cost is scaled by $1/s$.

3.4. Reduction Schedule

In addition to asymmetric redundancy mentioned in Sec. 3.2, Fig. 1 also reveals that perturbations in Q across the shallow, intermediate, and deep blocks lead to varying degradation patterns. Similarly, perturbations at different denoising timesteps exhibit comparable variations in degradation behavior. This raises a natural question: how does redundancy in the attention feature evolve across different blocks and denoising timesteps?

We examined intra-sequence similarity across blocks and timesteps in CogVideoX [65]. Fig. 5 illustrates temporal trends in similarity across blocks: 1) During the initial timesteps when the input to the denoising network closely resembles random noise, higher similarity is observed across different blocks; 2) As the generation progresses, the similarity generally decreases and stabilizes; 3) The temporal trends vary significantly between blocks. For instance, in the shallow blocks, the similarity of V increases steadily after the first ten steps. Whereas in other blocks, it remains relatively constant, forming a near-horizontal line.

Having made these observations, we can prioritize reducing computation for high-similarity blocks and timesteps while retaining low-similarity components to balance efficiency and generation quality. In practice, we precompute the content-agnostic similarity distribution for each model based on one arbitrary generation. This distribution is then used to estimate where and when reductions should occur.

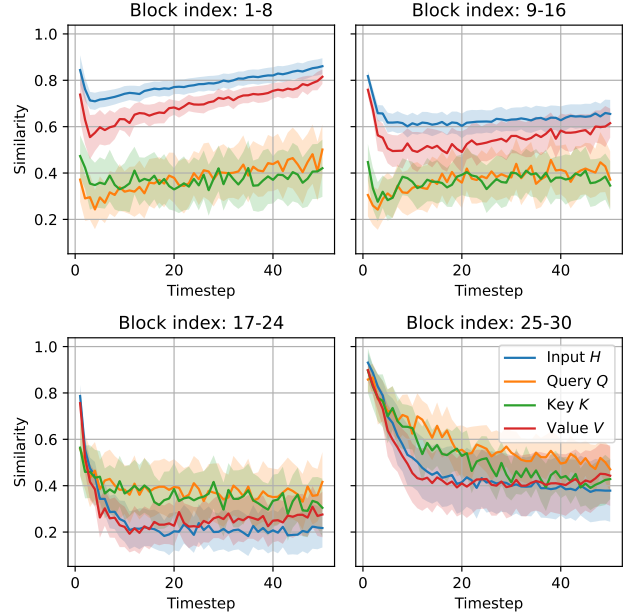


Figure 5. **Video DiT attention feature similarity.** Similarity values are standardized to $[0, 1]$ for visualization. The shaded areas indicate the confidence interval. Blocks are divided into four groups, each exhibiting distinct trends, with variations observed across different feature types. These patterns remain consistent across different objects, themes, and topics.

For example, the top 60% of the most similar parts of Q can undergo reduction, while the remaining 40% are left unmodified.

4. Experiments

To analyze the effects of AsymRnR, we conduct experiments on the text-to-video generation task. The implementation is introduced in Sec. 4.1, while we evaluate the generation latency, quality, and visualization in Sec. 4.2. And Sec. 4.3 analyzes the design choices of our approach.

4.1. Implementation Details

Our experiments use state-of-the-art open-source 3D DiT-based video generation models: CogVideoX 2B (CVX-2B) and 5B (CVX-5B) [65]. The generation uses the 50-step DDIM solver [48] from the original codebase, with 49 frames and a resolution of 480×720 . We focus on token reduction-based training-free inference time acceleration through token reduction techniques, using ToMe [3] as the baseline. To adapt ToMe to video scenario, we employ a 3D partition with a $2 \times 2 \times 2$ stride for consistency, aligning our setup mentioned in Sec. 3.1. Notably, the CVX-5B model incorporates 3D rotary position embeddings (ROPE) [51] in all layers' Q and K . ToMe reduction on input H is incompatible with this setting, so we only report metrics for

Method	FLOPs ($\times 10^{15}$)	Latency (second)	Speedup	VBench \uparrow
CVX-2B	12.000	137.30	-	0.8008
+ ToMe	10.549	123.59	1.11 \times	0.7825
+ ToMe-fast	10.120	118.26	1.16 \times	0.7732
+ Ours	10.342	121.70	1.13 \times	0.7917
+ Ours-fast	9.976	117.29	1.17\times	<u>0.7849</u>
CVX-5B	33.220	347.50	-	0.8074
+ ToMe	-	-	-	-
+ Ours	29.876	316.12	1.10 \times	0.8061
+ Ours-fast	29.190	308.86	1.13\times	0.8056

Table 1. **Quantitative evaluation of performance and latency.** FLOPs represent the floating-point operations required per video generation (with classifier-free guidance [17]). Speedup is calculated as $\Delta\text{latency}/\text{latency} + 1$. Video specifications: resolution 480×720 and 49 frames at 50 DDIM [48] steps.

CVX-2B. In contrast, AsymRnR reduces after the ROPE and does not encounter this issue.

We report the VBench [21] total score based on over 900 generated videos. Additionally, we provide FLOPs, latency, and speedup as efficiency metrics. Other automated metrics, such as SSIM [61] and PSNR, are not suitable for evaluation because high quality does not necessarily require pixel-wise alignment, as demonstrated in the visualization in Fig. 6. The latency is measured on an NVIDIA A100 40GB GPU using PyTorch v2.1.0. Memory-efficient attention [40] is enabled by default in all experiments.

4.2. Main Results

Both ToMe and AsymRnR can adjust latency by modifying the reduction rate r . We compare two configurations: a base version to ensure near-lossless quality from a human perception perspective, and a fast version for quicker generation with slight quality degradation. The reduction rate is manually tuned to align the latencies of both methods.

Quantitative Results. Tab. 1 presents the qualitative evaluation of the standard VBench text-to-video prompts suite [21]. For CVX-2B, our AsymRnR outperforms ToMe in VBench scores, even when comparing our fast configuration to ToMe’s base configuration, while also offering an extra 6-second speedup. When applied to CVX-5B, our method achieves a 1.13 \times speedup (39 seconds) with minimal impact on the VBench score, indicating the potential for lossless acceleration in larger models.

Qualitative Results. Fig. 6 presents a qualitative comparison on CVX-2B and CVX-5B. The results are evaluated against ToMe using the fast configuration detailed in Tab. 1. While the generated outputs are not pixel-wise aligned with the baselines, their overall quality remains high and comparable. In contrast, ToMe produces outputs that appear pixelated

Feature	Schedule	FLOPs ($\times 10^{15}$)	Latency (second)	VBench \uparrow
Q		10.204	123.42	0.7641
V		10.276	122.34	0.7765
Q	\checkmark	10.620	123.59	<u>0.7893</u>
V	\checkmark	10.403	122.19	0.7787
$Q + V$	\checkmark	10.342	121.70	0.7917

Table 2. **Performance improvements with the schedule.** With the reduction schedule, the reductions in Q and V demonstrate significant improvements without increasing latency, particularly for Q . Collaboratively reducing Q and V further improves performance while maintaining the same latency. Our default configurations are marked in blue.

and blurry.

4.3. Ablation Study

Quality-Latency Trade-off for Individual Features. Fig. 7 illustrates the quality-latency trade-off for features H , Q , K , and V . We observe that reducing individual features without the reduction schedule (discussed in Sec. 3.4) leads to a performance hierarchy: $V > H > K \gg Q$. Since K and V must share the same reduction behavior due to their one-to-one correspondence in the attention mechanism, we use the matching of V tokens to determine that of both K and V . Moreover, Q exhibits the most significant performance degradation as the reduction rate increases, a trend consistent with the observations in Fig. 1.

Reduction Schedule. Tab. 2 compares AsymRnR performance with and without the reduction schedule. With a capped budget (*i.e.* fixed latency), following the schedule to adjust reducible blocks and timesteps substantially enhances performance. Moreover, the improvement in Q surpasses V , suggesting that Q is more sensitive to interventions in low-redundancy blocks and timesteps but exhibits greater robustness to substantial reductions in high-redundancy regions. Specifically, reducing the high-similarity parts of Q by 80% causes no perceptible artifacts in human evaluations, whereas reducing the low-similarity parts by just 10% results in noticeable blurriness and distortions. It underscores the necessity of implementing such a reduction schedule.

Notably, the reductions of Q and V do not conflict. Their collaborative reduction further enhances performance with the same latency.

Combining SymRnR and AsymRnR. A key question is whether increasing the reduction rate or further reducing additional features is more effective in squeezing the latency. We investigate the inclusion of the H , *i.e.* SymRnR. To prevent multiple reductions in the same region by SymRnR and AsymRnR, we integrate them in parallel: if a block is identi-

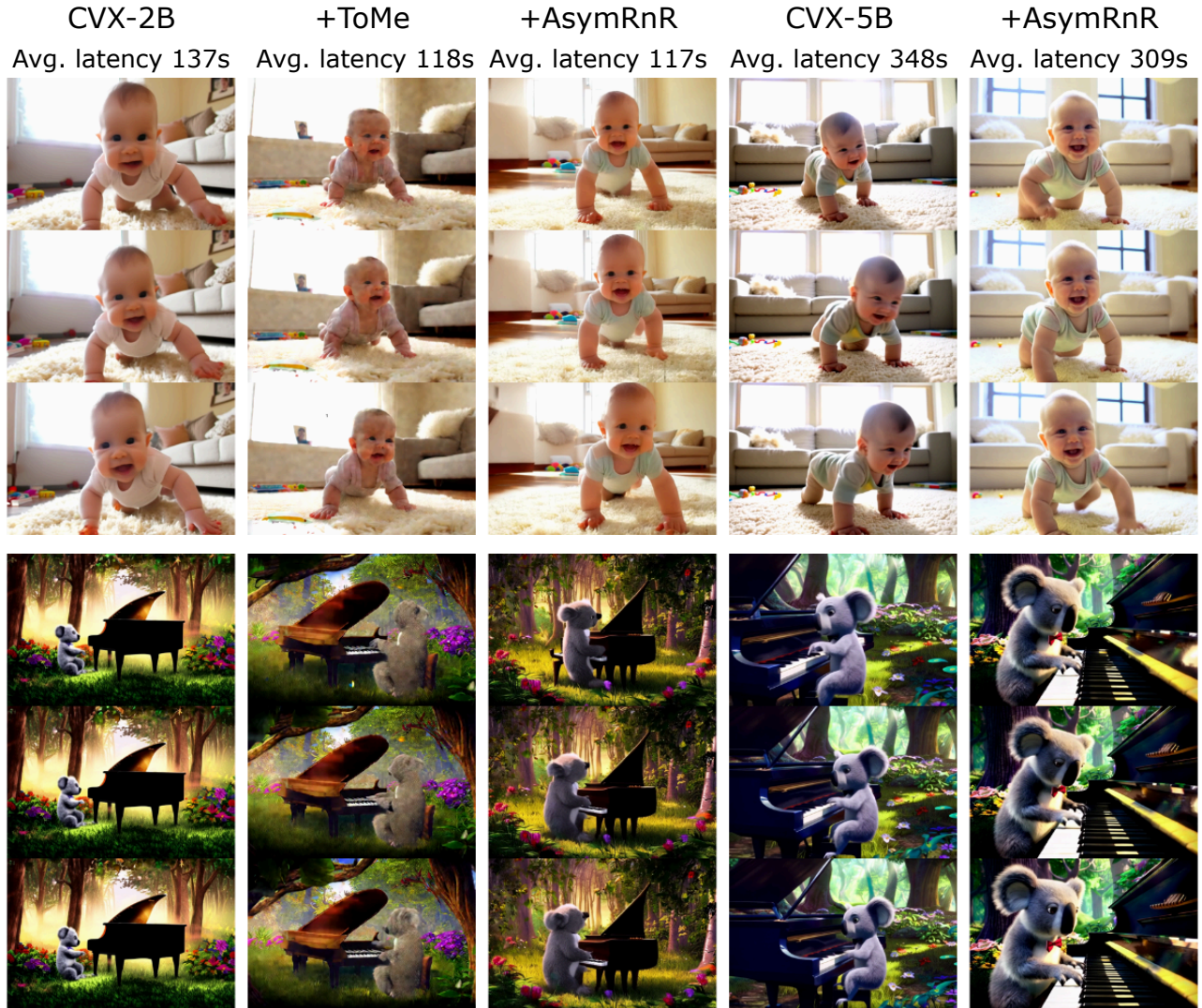


Figure 6. **Qualitative comparison.** Visualization of video quality generated by the baseline, ToMe, and AsymRnR (ours).

Feature	FLOPs ($\times 10^{15}$)	Latency (second)	VBench \uparrow
-	12.000	137.30	0.8008
$Q + V$	9.9755	117.29	0.7849
$H + Q + V$	10.0404	117.23	0.7766

Table 3. **Comparison of additional reduction rates and features.** Simply scaling the reduction rate outperforms the inclusion of H and SymRnR for lower latency.

fied as redundant in Q or V at a given timestep, the reduction will prioritize AsymRnR; if any part remains unreduced by AsymRnR and redundancy is identified by H , SymRnR can then reduce it. The performance of this parallelized Sym-

RnR + AsymRnR is displayed in the last row of Tab. 3. We also explore directly increasing the reduction rate of AsymRnR to match the latency of the parallelized configuration. The results on VBench indicate that incorporating additional reducible regions through SymRnR leads to worse performance than simply scaling AsymRnR.

Matching Cache. One major bottleneck affecting the latency of RnR is the matching stage. Our newly proposed matching cache reduces the matching cost by a factor of $1/s$, but may intuitively result in a potential performance degradation. Tab. 4 presents the performance across various caching steps. As the caching step increases from 0, both FLOPs and latency exhibit significant reductions, particularly at smaller values of s . However, the performance degradation is relatively minor, enabling us to adopt $s = 4$ as

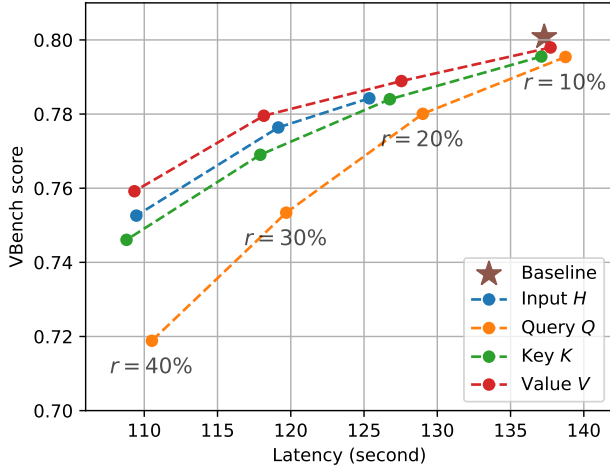


Figure 7. **Performance-latency trade-off for individual features.** We present the quality vs. latency curve for varying reduction ratios of ToMe [3] and other individual features on VBench [21], without employing the scheduler. Notably, reducing V alone consistently outperforms ToMe, which reduces H . However, reducing Q in isolation leads to a significant drop in performance, consistent with the trends observed in Fig. 1.

Cache s	FLOPs ($\times 10^{15}$)	Latency (second)	VBench \uparrow
-	12.000	137.30	0.8008
0	10.210	134.68	0.7859
1	10.161	124.24	<u>0.7822</u>
2	9.968	120.77	0.7798
3	9.943	118.61	0.7763
4	<u>9.917</u>	<u>118.16</u>	0.7796
5	9.909	117.51	0.7747

Table 4. **The effect of matching cache.** Calculating matching at each block and step ($s = 0$) provides minor acceleration with a moderate reduction rate ($r = 0.3$). Increasing the caching steps does not significantly degrade performance but reduces latency when $s < 5$. To isolate the impact of caching steps, this evaluation focuses solely on reducing V without employing a scheduler.

the default configuration, balancing latency and performance effectively.

Similarity Metric and Reduction Operator. Tab. 5 supports the conclusion from Sec. 3.2 that the default cosine similarity is suboptimal for handling long-tailed features in DiT. Euclidean similarity resolves this issue by accounting for both the direction and magnitude of tokens. Furthermore, while ToMe’s default mean reduction operation does not impact FLOPs, it introduces additional latency and negatively affects generation quality, leading to blurriness and distortion. By default, we simply discard redundant tokens,

Similarity	Reduction	FLOPs ($\times 10^{15}$)	Latency (second)	VBench \uparrow
random	discard	9.843	113.79	0.7112
dot	discard	9.914	117.92	0.7395
cosine	discard	9.914	118.08	0.7716
euclidean	discard	9.917	118.16	0.7796
euclidean	mean	9.917	119.90	0.7630

Table 5. **Comparison of similarity metrics and reduction operations.** The cosine similarity in ToMe [4] is suboptimal compared to Euclidean similarity for AsymRnR. Additionally, the averaging reduction operation introduces extra processing time and degrades performance due to increased blurriness and distortion. Directly discarding redundant tokens yields the best results.

Stride (t, h, w)	Destination r_d (%)	FLOPs ($\times 10^{15}$)	Latency (second)	VBench \uparrow
(1, 2, 2)	24.44%	9.979	123.60	<u>0.7624</u>
(2, 2, 2)	11.28%	9.917	118.16	0.7796
(3, 2, 2)	7.52%	9.894	115.66	0.7417
(4, 2, 2)	5.64%	<u>9.882</u>	<u>114.55</u>	0.7356
(2, 3, 3)	5.13%	<u>9.879</u>	<u>114.10</u>	0.7372
(2, 4, 4)	2.63%	9.862	112.58	0.7231

Table 6. **Destination partition stride and ratio.** An excessively large portion of destination tokens increases latency, while a smaller portion degrades performance. A stride of (2, 2, 2) strikes a balance between the two.

resulting in improved performance.

Destination Partition. The partitioning of source and destination tokens during matching significantly impacts final performance. The similarity calculation of BSM has a complexity proportional to $r_d(1 - r_d)n^2$, which increases monotonically for $0 < r_d < 1/2$, where r_d represents the fraction of destination tokens, and n is the total number of tokens. As shown in Table 1, a small r_d leads to drastic performance degradation due to less accurate matching results. Conversely, a larger r_d slightly worsens performance and increases latency because of reduced temporal regularization. We adopt a stride configuration of (2, 2, 2) as the default.

5. Discussion

Limitation. AsymRnR is a training-free acceleration approach compatible with various DiT models. However, its generation quality and speedup are influenced by the specific baseline models. Any inherent biases or limitations of the baseline models are also inherited. While the generation quality remains robust without noticeable degradation, the generated content may deviate slightly from the baseline method, even when the random seed is controlled.

Further study. The performance of the AsymRnR is cur-

rently limited by the training-free paradigm. Future work can focus on parameter-efficient fine-tuning techniques to enhance acceleration capabilities. While our method is inherently compatible with distillation-based and feature-caching approaches, this paper does not explore their integration due to the lack of publicly available solutions tailored to the 3D video DiT architecture. Further investigations into these integrations are warranted to maximize the method’s applicability and efficiency.

6. Conclusion

This paper presents AsymRnR, a training-free approach for lossless acceleration of video DiTs. It adaptively accelerates computation by non-uniformly allocating reduced operations across attention features, blocks, and denoising steps, leveraging the inherent redundancy in video DiTs. To further enhance efficiency, we introduce a matching cache mechanism that minimizes matching overhead, ensuring that acceleration gains are fully realized. Applied to state-of-the-art video DiTs in comprehensive experiments, our approach achieves significant speedups while maintaining output quality. These results highlight the potential of AsymRnR to drive practical efficiency improvements in video generation.

References

- [1] Lei Jimmy Ba, Jamie Ryan Kiros, and Geoffrey E. Hinton. Layer normalization. *CoRR*, abs/1607.06450, 2016. [2](#)
- [2] Yogesh Balaji, Seungjun Nah, Xun Huang, Arash Vahdat, Jiaming Song, Karsten Kreis, Miika Aittala, Timo Aila, Samuli Laine, Bryan Catanzaro, Tero Karras, and Ming-Yu Liu. ediff-i: Text-to-image diffusion models with an ensemble of expert denoisers. *CoRR*, abs/2211.01324, 2022. [4](#)
- [3] Daniel Bolya and Judy Hoffman. Token merging for fast stable diffusion. In *CVPR Workshops*, pages 4599–4603. IEEE, 2023. [1](#), [2](#), [3](#), [4](#), [5](#), [8](#)
- [4] Daniel Bolya, Cheng-Yang Fu, Xiaoliang Dai, Peizhao Zhang, Christoph Feichtenhofer, and Judy Hoffman. Token merging: Your vit but faster. In *ICLR*. OpenReview.net, 2023. [3](#), [4](#), [5](#), [8](#)
- [5] Junsong Chen, Jincheng Yu, Chongjian Ge, Lewei Yao, Enze Xie, Zhongdao Wang, James T. Kwok, Ping Luo, Huchuan Lu, and Zhenguo Li. Pixart- α : Fast training of diffusion transformer for photorealistic text-to-image synthesis. In *ICLR*. OpenReview.net, 2024. [2](#)
- [6] Pengtao Chen, Mingzhu Shen, Peng Ye, Jianjian Cao, Chongjun Tu, Christos-Savvas Bouganis, Yiren Zhao, and Tao Chen. Δ -dit: A training-free acceleration method tailored for diffusion transformers. *CoRR*, abs/2406.01125, 2024. [3](#), [4](#)
- [7] Rohan Choudhury, Guanglei Zhu, Sihan Liu, Koichiro Niinuma, Kris M Kitani, and László Jeni. Don’t look twice: Faster video transformers with run-length tokenization. *CoRR*, abs/2411.05222, 2024. [3](#)
- [8] Tri Dao. Flashattention-2: Faster attention with better parallelism and work partitioning. In *ICLR*. OpenReview.net, 2024. [1](#), [2](#)
- [9] Tri Dao, Daniel Y. Fu, Stefano Ermon, Atri Rudra, and Christopher Ré. Flashattention: Fast and memory-efficient exact attention with io-awareness. In *NeurIPS*, 2022. [1](#), [2](#)
- [10] Timothée Darcet, Maxime Oquab, Julien Mairal, and Piotr Bojanowski. Vision transformers need registers. In *ICLR*. OpenReview.net, 2024. [3](#)
- [11] Tim Dockhorn, Arash Vahdat, and Karsten Kreis. GENIE: higher-order denoising diffusion solvers. In *NeurIPS*, 2022. [2](#)
- [12] Yihe Dong, Jean-Baptiste Cordonnier, and Andreas Loukas. Attention is not all you need: Pure attention loses rank doubly exponentially with depth. *CoRR*, abs/2103.03404, 2021. [4](#)
- [13] Abhimanyu Dubey, Abhinav Jauhri, Abhinav Pandey, and et al. The llama 3 herd of models. *CoRR*, abs/2407.21783, 2024. [2](#)
- [14] Patrick Esser, Sumith Kulal, Andreas Blattmann, Rahim Entezari, Jonas Müller, Harry Saini, Yam Levi, Dominik Lorenz, Axel Sauer, Frederic Boesel, Dustin Podell, Tim Dockhorn, Zion English, and Robin Rombach. Scaling rectified flow transformers for high-resolution image synthesis. In *ICML*. OpenReview.net, 2024. [2](#)
- [15] Yuwei Guo, Ceyuan Yang, Anyi Rao, Zhengyang Liang, Yao-hui Wang, Yu Qiao, Maneesh Agrawala, Dahua Lin, and Bo Dai. Animatediff: Animate your personalized text-to-image diffusion models without specific tuning. In *ICLR*. OpenReview.net, 2024. [2](#)
- [16] Amirhossein Habibian, Amir Ghodrati, Noor Fathima, Guillaume Sautière, Risheek Garrepalli, Fatih Porikli, and Jens Petersen. Clockwork diffusion: Efficient generation with model-step distillation. In *CVPR*, pages 8352–8361. IEEE, 2024. [3](#)
- [17] Jonathan Ho and Tim Salimans. Classifier-free diffusion guidance. *CoRR*, abs/2207.12598, 2022. [6](#)
- [18] Jonathan Ho, Ajay Jain, and Pieter Abbeel. Denoising diffusion probabilistic models. In *NeurIPS*, 2020. [1](#)
- [19] Jonathan Ho, Tim Salimans, Alexey A. Gritsenko, William Chan, Mohammad Norouzi, and David J. Fleet. Video diffusion models. In *NeurIPS*, 2022. [2](#)
- [20] Edward J. Hu, Yelong Shen, Phillip Wallis, Zeyuan Allen-Zhu, Yuanzhi Li, Shean Wang, Lu Wang, and Weizhu Chen. Lora: Low-rank adaptation of large language models. In *ICLR*. OpenReview.net, 2022. [3](#)
- [21] Ziqi Huang, Yanan He, Jiashuo Yu, Fan Zhang, Chenyang Si, Yuming Jiang, Yuanhan Zhang, Tianxing Wu, Qingyang Jin, Nattapol Chanpaisit, Yaohui Wang, Xinyuan Chen, Limin Wang, Dahua Lin, Yu Qiao, and Ziwei Liu. Vbench: Comprehensive benchmark suite for video generative models. In *CVPR*, pages 21807–21818. IEEE, 2024. [6](#), [8](#)
- [22] Yatai Ji, Rongcheng Tu, Jie Jiang, Weijie Kong, Chengfei Cai, Wenzhe Zhao, Hongfa Wang, Yujiu Yang, and Wei Liu. Seeing what you miss: Vision-language pre-training with semantic completion learning. In *IEEE/CVF Conference on Computer Vision and Pattern Recognition, CVPR 2023, Vancouver, BC, Canada, June 17-24, 2023*, pages 6789–6798. IEEE, 2023. [3](#)
- [23] Kumara Kahatapitiya, Adil Karjauv, Davide Abati, Fatih Porikli, Yuki M. Asano, and Amirhossein Habibian. Object-centric diffusion for efficient video editing. In *ECCV (57)*, pages 91–108. Springer, 2024. [2](#), [3](#), [4](#)

- [24] Kumara Kahatapitiya, Haozhe Liu, Sen He, Ding Liu, Menglin Jia, Michael S Ryoo, and Tian Xie. Adaptive caching for faster video generation with diffusion transformers. *CoRR*, abs/2411.02397, 2024. 1, 3
- [25] Yoon Kim, Carl Denton, Luong Hoang, and Alexander M. Rush. Structured attention networks. In *ICLR (Poster)*. OpenReview.net, 2017. 4
- [26] Rajat Koner, Gagan Jain, Prateek Jain, Volker Tresp, and Sujoy Paul. Lookupvit: Compressing visual information to a limited number of tokens. In *ECCV (86)*, pages 322–337. Springer, 2024. 3
- [27] PKU-Yuan Lab and Tuzhan AI etc. Open-sora-plan, 2024. 1, 2
- [28] Yaniv Leviathan, Matan Kalman, and Yossi Matias. Selective attention improves transformer. *CoRR*, abs/2410.02703, 2024. 3
- [29] Xirui Li, Chao Ma, Xiaokang Yang, and Ming-Hsuan Yang. Vidtime: Video token merging for zero-shot video editing. In *CVPR*, pages 7486–7495. IEEE, 2024. 1, 2, 3, 4
- [30] Xingchao Liu, Chengyue Gong, and Qiang Liu. Flow straight and fast: Learning to generate and transfer data with rectified flow. In *ICLR*. OpenReview.net, 2023. 3
- [31] Xingchao Liu, Xiwen Zhang, Jianzhu Ma, Jian Peng, and Qiang Liu. InstafLOW: One step is enough for high-quality diffusion-based text-to-image generation. In *ICLR*. OpenReview.net, 2024. 3
- [32] Cheng Lu, Yuhao Zhou, Fan Bao, Jianfei Chen, Chongxuan Li, and Jun Zhu. Dpm-solver: A fast ODE solver for diffusion probabilistic model sampling in around 10 steps. In *NeurIPS*, 2022. 2
- [33] Simian Luo, Yiqin Tan, Longbo Huang, Jian Li, and Hang Zhao. Latent consistency models: Synthesizing high-resolution images with few-step inference. *CoRR*, abs/2310.04378, 2023. 3
- [34] Simian Luo, Yiqin Tan, Suraj Patil, Daniel Gu, Patrick von Platen, Apolinário Passos, Longbo Huang, Jian Li, and Hang Zhao. Lcm-lora: A universal stable-diffusion acceleration module. *CoRR*, abs/2311.05556, 2023. 1, 3
- [35] Xinyin Ma, Gongfan Fang, and Xinchao Wang. Deepcache: Accelerating diffusion models for free. In *CVPR*, pages 15762–15772. IEEE, 2024. 3, 4
- [36] Xin Ma, Yaohui Wang, Gengyun Jia, Xinyuan Chen, Ziwei Liu, Yuan-Fang Li, Cunjian Chen, and Yu Qiao. Latte: Latent diffusion transformer for video generation. *CoRR*, abs/2401.03048, 2024. 1, 2
- [37] Zi-Ao Ma, Tian Lan, Rong-Cheng Tu, Yong Hu, Heyan Huang, and Xian-Ling Mao. Multi-modal retrieval augmented multi-modal generation: A benchmark, evaluate metrics and strong baselines. *CoRR*, abs/2411.16365, 2024. 3
- [38] Chenlin Meng, Robin Rombach, Ruiqi Gao, Diederik P. Kingma, Stefano Ermon, Jonathan Ho, and Tim Salimans. On distillation of guided diffusion models. In *CVPR*, pages 14297–14306. IEEE, 2023. 1, 2
- [39] William Peebles and Saining Xie. Scalable diffusion models with transformers. In *ICCV*, pages 4172–4182. IEEE, 2023. 1
- [40] Markus N. Rabe and Charles Staats. Self-attention does not need $o(n^2)$ memory. *CoRR*, abs/2112.05682, 2021. 1, 2, 6
- [41] Yongming Rao, Wenliang Zhao, Benlin Liu, Jiwen Lu, Jie Zhou, and Cho-Jui Hsieh. Dynamicvit: Efficient vision transformers with dynamic token sparsification. In *NeurIPS*, pages 13937–13949, 2021. 1, 3
- [42] Robin Rombach, Andreas Blattmann, Dominik Lorenz, Patrick Esser, and Björn Ommer. High-resolution image synthesis with latent diffusion models. In *CVPR*, pages 10674–10685. IEEE, 2022. 2, 3
- [43] Olaf Ronneberger, Philipp Fischer, and Thomas Brox. U-net: Convolutional networks for biomedical image segmentation. In *MICCAI (3)*, pages 234–241. Springer, 2015. 2, 3
- [44] Tim Salimans and Jonathan Ho. Progressive distillation for fast sampling of diffusion models. In *ICLR*. OpenReview.net, 2022. 1, 2
- [45] Axel Sauer, Dominik Lorenz, Andreas Blattmann, and Robin Rombach. Adversarial diffusion distillation. In *ECCV (86)*, pages 87–103. Springer, 2024. 1, 3
- [46] Xincheng Shuai, Henghui Ding, Xingjun Ma, Rongcheng Tu, Yu-Gang Jiang, and Dacheng Tao. A survey of multimodal-guided image editing with text-to-image diffusion models. *CoRR*, abs/2406.14555, 2024. 1
- [47] Jascha Sohl-Dickstein, Eric A. Weiss, Niru Maheswaranathan, and Surya Ganguli. Deep unsupervised learning using nonequilibrium thermodynamics. In *ICML*, pages 2256–2265. JMLR.org, 2015. 1
- [48] Jiaming Song, Chenlin Meng, and Stefano Ermon. Denoising diffusion implicit models. In *ICLR*. OpenReview.net, 2021. 2, 5, 6
- [49] Yang Song and Stefano Ermon. Generative modeling by estimating gradients of the data distribution. In *NeurIPS*, pages 11895–11907, 2019. 1
- [50] Yang Song, Prafulla Dhariwal, Mark Chen, and Ilya Sutskever. Consistency models. *CoRR*, abs/2303.01469, 2023. 3
- [51] Jianlin Su, Murat H. M. Ahmed, Yu Lu, Shengfeng Pan, Wen Bo, and Yunfeng Liu. Roformer: Enhanced transformer with rotary position embedding. *Neurocomputing*, 568:127063, 2024. 2, 5
- [52] Wenhao Sun, Rong-Cheng Tu, Jingyi Liao, and Dacheng Tao. Diffusion model-based video editing: A survey. *CoRR*, abs/2407.07111, 2024. 1
- [53] Genmo Team. Mochi 1: A new sota in open-source video generation models. <https://www.genmo.ai/blog>, 2024. Accessed: 2024-11-20. 1, 2
- [54] Hunyuan Foundation Model Team. Hunyuanvideo: A systematic framework for large video generative models. *CoRR*, abs/2412.03603, 2024. 1
- [55] Movie Gen Team. Movie gen: A cast of media foundation models. <https://ai.meta.com/research/publications/movie-gen-a-cast-of-media-foundation-models/>, 2024. Accessed: 2024-11-20. 2
- [56] Rong-Cheng Tu, Yatai Ji, Jie Jiang, Weijie Kong, Chengfei Cai, Wenzhe Zhao, Hongfa Wang, Yujiu Yang, and Wei Liu. Global and local semantic completion learning for vision-language pre-training. *CoRR*, abs/2306.07096, 2023. 3

- [57] Rong-Cheng Tu, Zi-Ao Ma, Tian Lan, Yuehao Zhao, Heyan Huang, and Xian-Ling Mao. Automatic evaluation for text-to-image generation: Task-decomposed framework, distilled training, and meta-evaluation benchmark. *CoRR*, abs/2411.15488, 2024. 3
- [58] Rong-Cheng Tu, Wenhao Sun, Zhao Jin, Jingyi Liao, Jiaying Huang, and Dacheng Tao. Spagent: Adaptive task decomposition and model selection for general video generation and editing. *CoRR*, abs/2411.18983, 2024. 1
- [59] Jiuniu Wang, Hangjie Yuan, Dayou Chen, Yingya Zhang, Xiang Wang, and Shiwei Zhang. Modelscope text-to-video technical report. *CoRR*, abs/2308.06571, 2023. 2
- [60] Yaohui Wang, Xinyuan Chen, Xin Ma, Shangchen Zhou, Ziqi Huang, Yi Wang, Ceyuan Yang, Yinan He, Jiashuo Yu, Peiqing Yang, Yuwei Guo, Tianxing Wu, Chenyang Si, Yuming Jiang, Cunjian Chen, Chen Change Loy, Bo Dai, Dahua Lin, Yu Qiao, and Ziwei Liu. LAVIE: high-quality video generation with cascaded latent diffusion models. *CoRR*, abs/2309.15103, 2023. 2
- [61] Zhou Wang, Alan C. Bovik, Hamid R. Sheikh, and Eero P. Simoncelli. Image quality assessment: from error visibility to structural similarity. *IEEE Trans. Image Process.*, 13(4): 600–612, 2004. 6
- [62] Felix Wimbauer, Bichen Wu, Edgar Schönfeld, Xiaoliang Dai, Ji Hou, Zijian He, Artsiom Sanakoyeu, Peizhao Zhang, Sam S. Tsai, Jonas Kohler, Christian Rupprecht, Daniel Cremers, Peter Vajda, and Jialiang Wang. Cache me if you can: Accelerating diffusion models through block caching. In *CVPR*, pages 6211–6220. IEEE, 2024. 3
- [63] Guangxuan Xiao, Jiaming Tang, Jingwei Zuo, Junxian Guo, Shang Yang, Haotian Tang, Yao Fu, and Song Han. Duoattention: Efficient long-context LLM inference with retrieval and streaming heads. *CoRR*, abs/2410.10819, 2024. 3
- [64] Zhen Xing, Qijun Feng, Haoran Chen, Qi Dai, Han Hu, Hang Xu, Zuxuan Wu, and Yu-Gang Jiang. A survey on video diffusion models. *ACM Comput. Surv.*, 57(2):41:1–41:42, 2025. 1
- [65] Zhuoyi Yang, Jiayan Teng, Wendi Zheng, Ming Ding, Shiyu Huang, Jiazheng Xu, Yuanming Yang, Wenyi Hong, Xiaohan Zhang, Guanyu Feng, Da Yin, Xiaotao Gu, Yuxuan Zhang, Weihang Wang, Yean Cheng, Ting Liu, Bin Xu, Yuxiao Dong, and Jie Tang. Cogvideox: Text-to-video diffusion models with an expert transformer. *CoRR*, abs/2408.06072, 2024. 1, 2, 5
- [66] Hongxu Yin, Arash Vahdat, José M. Álvarez, Arun Mallya, Jan Kautz, and Pavlo Molchanov. A-vit: Adaptive tokens for efficient vision transformer. In *CVPR*, pages 10799–10808. IEEE, 2022. 1, 3
- [67] Lijun Yu, José Lezama, Nitesh Bharadwaj Gundavarapu, Luca Versari, Kihyuk Sohn, David Minnen, Yong Cheng, Agrim Gupta, Xiuye Gu, Alexander G. Hauptmann, Boqing Gong, Ming-Hsuan Yang, Irfan Essa, David A. Ross, and Lu Jiang. Language model beats diffusion - tokenizer is key to visual generation. In *ICLR*. OpenReview.net, 2024. 2
- [68] Chenshuang Zhang, Chaoning Zhang, Mengchun Zhang, and In So Kweon. Text-to-image diffusion models in generative AI: A survey. *CoRR*, abs/2303.07909, 2023. 1
- [69] David Junhao Zhang, Jay Zhangjie Wu, Jia-Wei Liu, Rui Zhao, Lingmin Ran, Yuchao Gu, Difei Gao, and Mike Zheng Shou. Show-1: Marrying pixel and latent diffusion models for text-to-video generation. *CoRR*, abs/2309.15818, 2023. 2
- [70] Qinsheng Zhang and Yongxin Chen. Fast sampling of diffusion models with exponential integrator. In *ICLR*. OpenReview.net, 2023. 2
- [71] Wentian Zhang, Haozhe Liu, Jinheng Xie, Francesco Faccio, Mike Zheng Shou, and Jürgen Schmidhuber. Cross-attention makes inference cumbersome in text-to-image diffusion models. *CoRR*, abs/2404.02747, 2024. 1, 3
- [72] Xuanlei Zhao, Xiaolong Jin, Kai Wang, and Yang You. Real-time video generation with pyramid attention broadcast. *CoRR*, abs/2408.12588, 2024. 1, 3
- [73] Zangwei Zheng, Xiangyu Peng, Tianji Yang, Chenhui Shen, Shenggui Li, Hongxin Liu, Yukun Zhou, Tianyi Li, and Yang You. Open-sora: Democratizing efficient video production for all, 2024. 1, 2